SEISMIC RESPONSE PREDICTION FOR TORSIONALLY IRREGULAR BUILDINGS USING STRUCTURAL HEALTH MONITORING AND MACHINE LEARNING

PREDICCIÓN DE LA RESPUESTA SÍSMICA DE EDIFICACIONES CON IRREGULARIDAD TORSIONAL EMPLEANDO EL MONITOREO DE LA SALUD ESTRUCTURAL Y APRENDIZAJE AUTOMÁTICO

Elvis Guizado[1*], Miguel Diaz[1,2], Sergio Isuhuaylas[1]

[1]Centro Peruano Japonés de Investigaciones Sísmicas y Mitigación de Desastres, Universidad Nacional de Ingeniería, Lima, Perú

[2]Facultad de Ingeniería Civil, Universidad Nacional de Ingeniería, Lima, Perú

Received (Recibido): 23 / 01 / 3000 Publicado (Published): 07/ 02 / 3001

ABSTRACT

Given the seismic risk that buildings in Peru face, monitoring the structural health of critical infrastructure is essential. Structural health monitoring (SHM) is commonly carried out at the center of mass (CM) of buildings using accelerometers. However, in torsional irregular structures, the maximum response does not occur at the CM due to the torsional effect produced by the existing in-plan eccentricity between the centers of stiffness (CS) and mass. This research proposes a methodology to estimate the maximum response in buildings with torsional effects using SHM with accelerometers positioned at the CM. In the proposed methodology, the degree of torsional irregularity was defined to enable the calculation of the maximum seismic response. Consequently, a new machine learning model for predicting the degree of torsional irregularity was developed using 9,358 seismic simulations. The prediction model achieved a normalized error of 4.054% in estimating the maximum seismic response. Likewise, incremental dynamic tests were carried out on a shaking table with 8 specimens having different structural configurations. The experimental results were used to assimilate the developed model with the numerical results, thus obtaining a hybrid prediction model for the degree of torsional irregularity. Finally, a mathematical expression was proposed to estimate the degree of torsional irregularity using experimental results based on the structural and seismic characteristics validated with the hybrid prediction model. The proposed methodology is important because this tool can provide a more accurate assessment of the state of torsional irregular structures after the occurrence of an earthquake.

Keywords: degree of torsional irregularity, structural health monitoring, maximum drift, numerical simulation, dynamic tests

RESUMEN

Dado el riesgo sísmico que enfrentan los edificios en Perú, el monitoreo de la salud estructural de la infraestructura crítica es esencial. El monitoreo de la salud estructural (SHM, por sus siglas en inglés) se realiza comúnmente en el centro de masa (CM) de los edificios utilizando acelerómetros. Sin embargo, en estructuras con irregularidad torsional, la respuesta máxima no ocurre en el CM debido al efecto de torsión producido por la excentricidad en planta existente entre los centros de rigidez (CS) y masa. Proponemos una metodología para estimar la respuesta máxima en edificios con efectos de torsión utilizando SHM con acelerómetros posicionados en el CM. En la metodología propuesta, se definió el grado de irregularidad torsional para permitir el cálculo de la respuesta sísmica máxima. En consecuencia, se desarrolló un nuevo modelo de aprendizaje automático para predecir el grado de irregularidad torsional utilizando 9,358 simulaciones sísmicas. El modelo de predicción alcanzó un error normalizado del 4.054% en la estimación de la respuesta sísmica máxima. Asimismo, se llevaron a cabo pruebas dinámicas incrementales en una mesa vibratoria con 8 especímenes que presentaban diferentes configuraciones estructurales. Los resultados experimentales se utilizaron para asimilar el modelo desarrollado con los resultados numéricos, obteniéndose así un modelo híbrido de predicción del grado de irregularidad torsional. Finalmente, se propuso una expresión matemática para estimar el grado de irregularidad torsional mediante resultados experimentales, basada en las características estructurales y sísmicas validadas con el modelo híbrido de predicción. La metodología propuesta es importante porque esta herramienta puede proporcionar una evaluación más precisa del estado de las estructuras con irregularidad torsional después de la ocurrencia de un sismo.

Palabras Clave: grado de irregularidad torsional, monitoreo de la salud estructural, distorsión máxima, simulación numérica, ensayos dinámicos

[1] * Corresponding author:
E-mail: elvis.guizado.c@uni.pe

1. INTRODUCTION

Buildings in Peru are exposed to a significant seismic threat due to the country's location on the Pacific Ring of Fire. Pulido et al. [1] estimate the occurrence of an M_w 8.9 magnitude earthquake on the central coast of Peru. Therefore, it is essential to have a continuous structural health monitoring system in place for essential buildings such as healthcare facilities and educational institutions, to understand the behavior and condition of these types of buildings immediately after the seismic event. In a study conducted by Ibrahim et al. [2], the idea is reinforce that continuous structural monitoring allows for rapid acquisition of information about a building's structural health after a seismic event. This enables rescue teams to prioritize assistance to the most vulnerable buildings, thus contributing to the prevention of human losses. In Peru, one of the institutions that performs continuous structural monitoring is the Japan-Peru Center for Earthquake Engineering Research and Disaster Mitigation (CISMID), which operates the Center for Earthquake Engineering Observation (CEOIS). The CEOIS is composed of three monitoring networks covering the entire Peruvian territory. Among these networks is the Building Monitoring Network (REMOED), which currently monitors several buildings throughout the country [3].

Gokdemir et al. [4] emphasize the importance of studying irregularities in structures, particularly torsional irregularities. The eccentricity between the center of mass of buildings and their center of stiffness causes structures to experience torsional effects during a seismic event. Under excessive torsional effects, elements can fail due to torsional moments, or the structure may exceed the limits of lateral deflection for which it was initially designed. Several studies, including those by Bozorgnia and Tso [5]; Chopra and Goel [6]; among others, have extensively investigated the impact of torsional irregularities on structural response. Findings from these studies consistently demonstrate that buildings with torsional irregularities are significantly more vulnerable to earthquake-induced damage. Observations from major seismic events—such as the 1985 Michoacán earthquake, the 1989 Loma Prieta earthquake, the 1994 Northridge earthquake, and the 1995 Kobe earthquake—have confirmed that many structures sustained severe damage attributable to torsional effects [7].

Finally, it is worth noting that machine learning algorithms have gained significant importance in recent times. They are now applied in the field of engineering, notably in structural dynamics. Oh et al. [8] used these algorithms to predict damage in structural models of buildings during seismic events. In this context, machine learning algorithms will be employed in present research as well.

2. BACKGROUND AND SCOPE

Structural health monitoring of buildings provides deeper insight into their behavior during seismic events. The installation of monitoring systems is particularly crucial in Peru due to seismic activity and the vulnerability of critical buildings such as hospitals and schools. In 2023, Jaramillo et al. [9] conducted a study on the dynamic behavior of an isolated building utilizing data obtained from monitoring sensors installed in the building to calculate the dynamic properties of the building in order to enable the calibration of a numerical model and subsequently the evaluation of its performance during seismic events.

Ortiz [10] studied the effect of the simultaneity of seismic components on structures exhibiting torsional irregularity. To do so, simplified numerical models with three degrees of freedom were analyzed, incorporating eccentricities in one direction and varying degrees of torsional irregularity. These models were subjected to real and synthetic earthquakes using time-history dynamic analysis. The results indicated amplification in the seismic response of the models due to torsional irregularity and the simultaneity of seismic components.

Due to the scarcity of experimental studies on structures with torsional irregularity, in 2021, Suzuki et al. [11] proposed a methodology for calculating displacement demands considering the nonlinear effects of torsion. In their research, they evaluated two reinforced concrete specimens with seven-storey torsional irregularity, both scaled down to 50%. These specimens were subjected to unidirectional seismic records on a shaking table at the Tainan laboratory in Taiwan.

On the other hand, in a study conducted by Oh et al. [8], a prediction model based on neural networks was developed to estimate the maximum seismic response in regular buildings. The model was designed to predict maximum floor interstory drift and maximum displacement, considering structural characteristics and seismic records as input parameters. For the development of the prediction algorithm, regular structural models with three, four, and six degrees of freedom were used, as well as a structural model of a reinforced concrete building. The predictions of the developed model showed high accuracy.

From the studies, it can be concluded that continuous monitoring of buildings using accelerometers is essential, particularly for structures with torsional irregularities. These structures are particularly susceptible to experiencing local amplifications in their seismic responses due to torsional effects. Additionally, it is important to note that there are not many experimental studies representing the seismic response of buildings with torsional irregularities in plan. Finally, it is relevant to mention that machine learning algorithms have demonstrated high accuracy in predicting the seismic response of structural models.

The main objective of this study is to develop a methodology that allows for estimating damage in buildings with torsional irregularities, considering their nonlinear response. To achieve this, numerous one-story buildings were analyzed through both numerical simulations and experimental tests. The effects of torsional irregularities on the seismic behavior of multi-story buildings are beyond the scope of this research.

3. DEGREE OF TORSINAL IRREGULARITY AND PERFORMANCE METRICS

3.1 DEGREE OF TORSIONAL IRREGULARITY (G_{it})

Structural health monitoring is typically conducted at the center of mass of buildings using accelerometers. However, due to torsional effects, the maximum response of structures is concentrated in areas away from this monitored point. This means that the maximum response cannot be directly measured. Considering that the response of the center of mass is known thanks to the monitoring systems, it is important to define an index that relates this response to the maximum response of the structure.

According to Ortiz [10], the degree of torsional irregularity is the ratio between the maximum in-plane displacement of a floor and the displacement of the center of mass. This index represents the amplification of the response caused by in-plane torsional effects. This index is defined in equation (1).

$$G_{it} = \frac{\Delta_{max}}{\Delta_{CM}} \quad (1)$$

According to equation (1), it can be deduced that if the value of G_{it} is calculated or determined, it is possible to estimate the maximum response. Therefore, this research will aim to develop an algorithm that allows for determining the value of G_{it} for different seismic scenarios, and subsequently, to estimate the maximum response value.

3.2 MODEL PERFORMANCE METRICS

To evaluate the performance of prediction models or algorithms, it is essential to use evaluation metrics that compare the original values y with the predicted values $\hat{y}$, some of which are presented below:

3.2.1 Root Mean Square Error (RMSE)

The Root Mean Square Error (RMSE) can be calculated using equation (2) [12]:

$$RMSE = \sqrt{\frac{1}{n}\sum_{i=1}^{n}(y^{(i)} - \hat{y}^{(i)})^2} \quad (2)$$

$y^{(i)}$: original or measured value.
$\hat{y}^{(i)}$: predicted or calculated value.

The Normalized RMSE (NRMSE) can also be calculated to express performance in percentage terms, using equation (3):

$$NRMSE = \left(\sqrt{\frac{1}{n}\sum_{i=1}^{n}(y^{(i)} - \hat{y}^{(i)})^2}\right)/w \quad (3)$$

w: data interval length, defined as $w = \max(y) - \min(y)$.

3.2.1 Coefficient of Determination (R^2)

The Coefficient of Determination, denoted as R^2, can be calculated using equation (4). R^2 values range from zero to one, where a value of one indicates that the predicted or computed data perfectly fits the original or measured data [12].

$$R^2 = 1 - \frac{SSE}{SST} \quad (4)$$

SSE: Sum of Squared Errors $\sum_{i=1}^{n}\left(y^{(i)} - \hat{y}^{(i)}\right)^2$.
SST: Total Sum of Squares or total variance $\sum_{i=1}^{n}\left(y^{(i)} - \mu_y\right)^2$.
μ_y: mean of the measured data.

4. NUMERICAL SIMULATION

In this section, a nonlinear dynamic analysis was performed on simplified models with eccentricity in one direction under different seismic events that occurred in Peru. Based on the results obtained from the numerical simulations, a database will be created in terms of structural and seismic characteristics.

4.1 SEISMIC RECORDS

In this study, 14 seismic events were considered as a basis. These events correspond to different years and regions of Peru (see TABLE I). Additionally, TABLE II presents the characteristics of the corresponding seismic records, including their Peak Ground Acceleration (PGA) and dominant frequency, the latter obtained through Fast Fourier Transform (FFT) analysis. In this study, the soil types at the seismic recording sites were not analyzed. Instead, the seismic records were characterized based on their predominant frequencies and PGAs.

TABLE I
Seismic records information

Event	Region	Station name	Event date
1	Lima	Parque de la Reserva	10/17/1966
2	Lima	Parque de la Reserva	05/31/1970
3	Lima	Parque de la Reserva	10/03/1974
4	Lima	Parque de la Reserva	04/29/1991
5	Moquegua	César Vizcarra Vargas	06/23/2001
6	Arequipa	Estación UNSA	07/07/2001
7	Tacna	Jorge Basadre Grohmann University	07/07/2001
8	Tacna	Jorge Basadre Grohmann University	06/13/2005
9	Moquegua	Cesar Vizcarra Vargas	06/13/2005
10	Arequipa	Estacion UNSA	06/13/2005
11	Callao	Dirección de Hidrografía y Navegación	08/15/2007
12	Ica	UNICA	08/15/2007
13	Lima	Casa Dr. Piqué	08/15/2007
14	Moquegua	César Vizcarra Vargas	04/01/2014

TABLE II
Seismic records features

Event	Region	PGA (g)		Predominant frequency (Hz)	
		EW	NS	EW	NS
1	Lima	0.19	0.27	10.14	3.03
2	Lima	0.10	0.11	2.73	2.73
3	Lima	0.19	0.16	3.31	3.27
4	Lima	0.03	0.03	17.68	1.29
5	Moquegua	0.28	0.25	1.04	1.39
6	Arequipa	0.13	0.12	2.49	1.51
7	Tacna	0.04	0.04	0.52	0.44
8	Tacna	0.08	0.09	3.37	2.88
9	Moquegua	0.06	0.07	3.51	4.77
10	Arequipa	0.07	0.07	2.48	1.83
11	Callao	0.09	0.08	0.85	0.78
12	Ica	0.29	0.42	1.46	0.33
13	Lima	0.07	0.07	8.63	6.92
14	Moquegua	0.06	0.04	0.91	1.10

g: acceleration due to gravity
PGA: peak ground acceleration

The variety of events considered is necessary to create a broad database for training the prediction model of the degree of torsional irregularity. Each seismic event consists of 2 horizontal acceleration records, making a total of 28 seismic signals. Additionally, using 10 amplification factors, 280 signals were generated from these 28 records to perform the dynamic analyses. The simultaneity of seismic components was not considered in this study; therefore, each horizontal component was treated as an independent record.

Since the goal is to understand the response of structures with torsional irregularities under multiple scenarios, the seismic records were scaled by 10 integer amplification factors (from 1 to 10) to modify their PGA, resulting in a total of 280 seismic signals.

4.2 SIMPLIFIED NUMERICAL MODELS

Thirty-six simplified numerical models were structured to represent a single-level reinforced concrete structure with two frames in the X and Y directions. To introduce eccentricity in the structural models, two different frames were considered in the Y direction for each model (see Fig. 1a). This approach induces eccentricity between the center of mass (CM) and the center of stiffness (CS) – the latter being the theoretical point where the structure's lateral stiffness is concentrated – resulting in an eccentricity e_x along the X direction, as depicted in Fig. 1b.

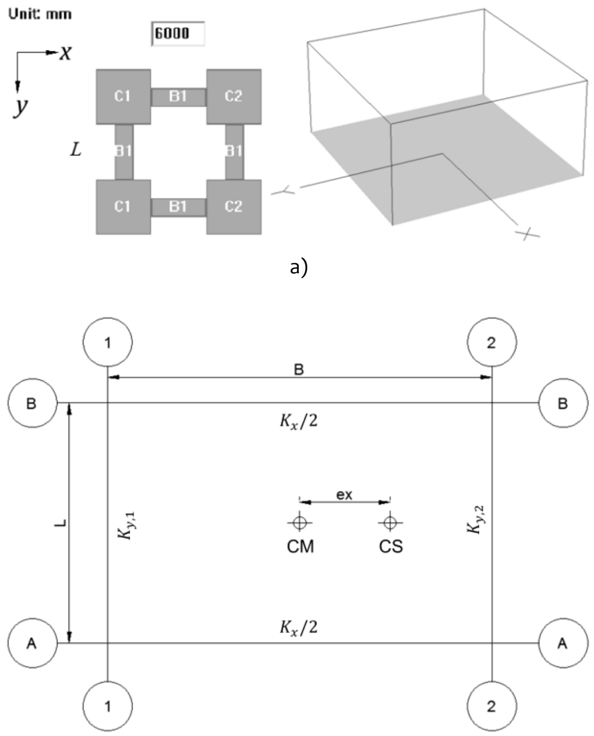

Fig. 1. Structural configuration of the simplified model. (a) Plan view and three-dimensional view of the structural elements of the simplified model. (b) Plan view of the eccentricity generated for the simplified model in the X direction.
$K_{y,1}$: stiffness of the structure in the Y direction along axis 1-1
$K_{y,2}$: stiffness of the structure in the Y direction along axis 2-2
K_x: stiffness of the structure in the X direction
e_x : eccentricity of the structure in the X direction

The dimensions of the 36 simplified models were defined with a constant width B=6 m and varying length L from 2.5 m to 6 m in increments of 0.1 m. To determine the sections of beams and columns, the maximum capacity of the models was analyzed using static nonlinear analysis. The goal was to achieve a

$$0.2 < \frac{Q_i}{W} < 0.6 \quad (5)$$

seismic coefficient for the models that satisfies the restriction of equation (5).

With the previous restriction, the dimensions and properties of the structural elements of the simplified models were defined (see TABLE III). Additionally, TABLE IV shows the plan dimensions of these models, as well as their seismic weights and respective seismic coefficients in the X and Y directions. It is important to highlight that the column depths are oriented along the Y-axis.

TABLE III
Properties of the structural elements of the simplified models

Element	b (m)	h (m)	$f'_c\left(\frac{kgf}{cm^2}\right)$	$f_y\left(\frac{kgf}{cm^2}\right)$
C1	0.30	0.30		
C2	0.30	0.60	280	4200
B1	0.30	0.60		

b: width of the element section
h: depth of the element section
f'_c: compressive strength of concrete
f_y: yield strength of reinforcing steel

TABLE IV
Characteristics of the simplified models

ID	B (m)	L (m)	Seismic Weight (kN)	$\frac{Q_{X,i}}{W}$	$\frac{Q_{Y,i}}{W}$
1	6.0	2.5	141.48	0.570	0.590
2	6.0	2.6	145.43	0.580	0.585
3	6.0	2.7	149.39	0.562	0.582
4	6.0	2.8	153.34	0.557	0.577
5	6.0	2.9	157.30	0.552	0.572
6	6.0	3.0	161.25	0.547	0.567
7	6.0	3.1	165.21	0.542	0.562
8	6.0	3.2	169.16	0.537	0.557
9	6.0	3.3	173.12	0.535	0.555
10	6.0	3.4	177.07	0.530	0.550
11	6.0	3.5	181.03	0.525	0.545
12	6.0	3.6	184.99	0.520	0.540
13	6.0	3.7	188.94	0.513	0.533
14	6.0	3.8	192.90	0.508	0.528
15	6.0	3.9	196.85	0.503	0.523
16	6.0	4.0	200.81	0.498	0.518
17	6.0	4.1	204.76	0.493	0.513
18	6.0	4.2	208.72	0.488	0.508
19	6.0	4.3	212.67	0.483	0.503
20	6.0	4.4	216.63	0.478	0.498
21	6.0	4.5	220.58	0.473	0.493
22	6.0	4.6	224.54	0.466	0.486
23	6.0	4.7	228.49	0.461	0.481
24	6.0	4.8	232.45	0.456	0.476
25	6.0	4.9	236.41	0.450	0.470
26	6.0	5.0	240.36	0.445	0.465
27	6.0	5.1	244.32	0.440	0.460
28	6.0	5.2	248.27	0.435	0.455
29	6.0	5.3	252.23	0.430	0.450
30	6.0	5.4	256.18	0.425	0.445
31	6.0	5.5	260.14	0.420	0.440
32	6.0	5.6	264.09	0.415	0.435
33	6.0	5.7	268.05	0.410	0.430
34	6.0	5.8	272.00	0.403	0.423
35	6.0	5.9	275.96	0.398	0.418
36	6.0	6.0	279.91	0.370	0.390

4.3 NONLINEAR TIME HISTORY ANALYSIS

The dynamic analyses were conducted using STERA 3D software, where the 36 models were subjected to the 280 seismic signals defined earlier. These signals were applied at three different incidence angles: 90°, 45°, and 30° measured relative to the positive X-axis. With these considerations, a total of 30,240 simulations were performed. This process is summarized in Fig. 2.

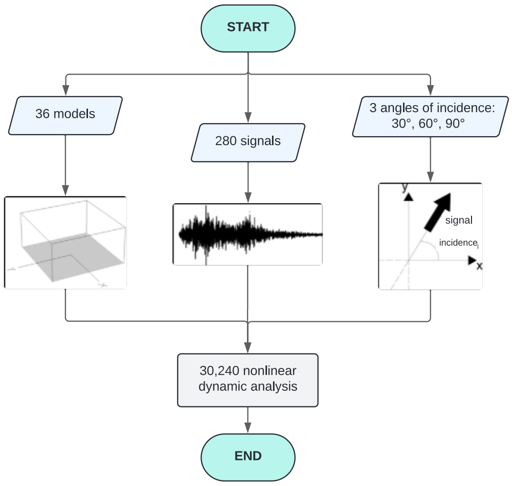

Fig. 2. Flowchart of Nonlinear Dynamic Analyses.

However, conducting 30,240 seismic analyses manually would require significant effort and be inefficient. Therefore, an algorithm was developed using Python to automate the execution of the analyses. The developed program modifies the input data (output result paths, plan dimensions and weights of the models, and seismic records) required by the STERA 3D software to perform nonlinear time history analysis. Fig. 3 shows the flowchart of the developed algorithm.

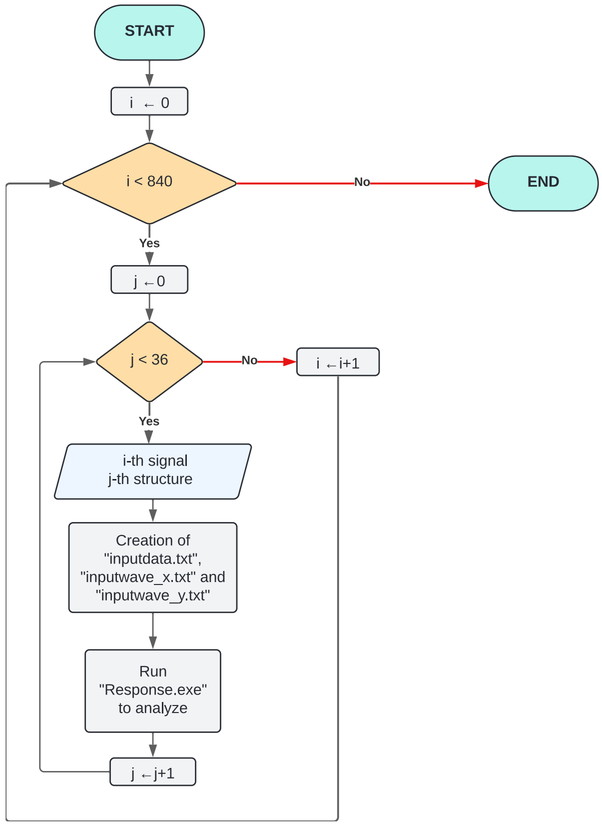

Fig. 3. Flowchart of the Python algorithm developed for the execution of dynamic analyses in STERA 3D.

After obtaining the results, they were filtered to consider only those that meet the following conditions (see filtering process in Fig. 4):

-Displacement of the center of mass in the Y direction less than 4.95 cm (1.5% drift). This consideration was made considering that Peruvian standard E030-2018 establishes a limit for drifts in reinforced concrete structures equal to 0.7%. It was decided to consider responses more adverse than this limit.
-Displacement of the center of mass in the Y direction greater than 0.33 cm (0.1% drift). This consideration aims to exclude cases with very small displacements since the focus is on studying the most adverse scenarios for the structures.
-A maximum ground acceleration threshold of less than 1g (9.81 m/s²) was adopted. This criterion was selected because, as shown in Table IV, the simplified models have seismic coefficients of up to 0.59g, indicating a potential for collapse under higher base accelerations. Nevertheless, ground motions with higher peak accelerations were also considered to evaluate the maximum nonlinear responses.

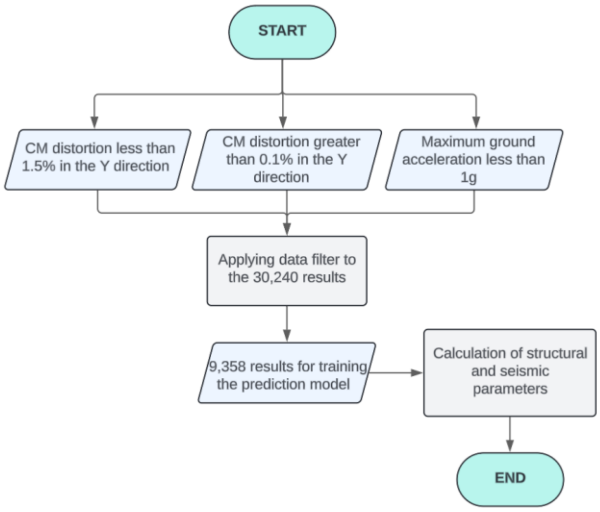

Fig. 4. Flowchart for data filtering.

After applying the filter, the number of results was reduced from 30,240 to 9,358. From these results, the structural and seismic parameters defined earlier will be calculated. Fig. 4 shows the histograms of the obtained parameters.

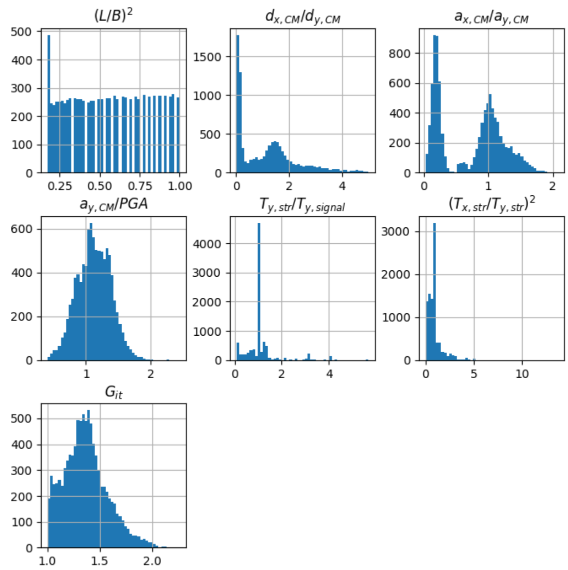

Fig. 5. Histograms of the structural and seismic parameters.

$d_{x,CM}$: Maximum displacement of the center of mass in the X direction.
$d_{y,CM}$: Maximum displacement of the center of mass in the Y direction.
$a_{x,CM}$: Maximum acceleration of the center of mass in the X direction.
$a_{y,CM}$: Maximum acceleration of the center of mass in the Y direction.
PGA_y: Peak ground acceleration in the Y direction.
$T_{x,str}$: Response period of the structure in the X direction.
$T_{y,str}$: Response period of the structure in the Y direction.
$T_{y,signal}$: Period of the seismic record in the Y direction.

5. EXPERIMENTAL PROGRAM

In this section, the development of the experimental process and its results will be presented. First, the structural configurations and details of the specimens tested on a shaking table will be shown. Next, the layout of the sensors installed for monitoring the structure's response will be presented. Finally, the results obtained from the monitoring system during incremental dynamic tests will be shown.

5.1 TEST SPECIMENS

Next, the floor plans of the test specimens will be shown. The tested specimens have been constructed using A36 steel parts, with a height of 45 cm, and dimensions of 60 cm width and length. Their total mass is approximately 70 kg. Fig. 6 shows the structural configuration of specimen E-1, which has a regular floor plan configuration. Additionally, the figure displays the natural frequency content of the free vibration of this specimen. The structural configurations of the other specimens will be derived from the configuration of specimen E-1, with modifications made to the corner columns N3 and N4 to increase stiffness along the axis connecting these columns in the Y direction. These variations were made considering that the vibrations from the shaking table to which the specimen will be subjected will occur in the Y direction.

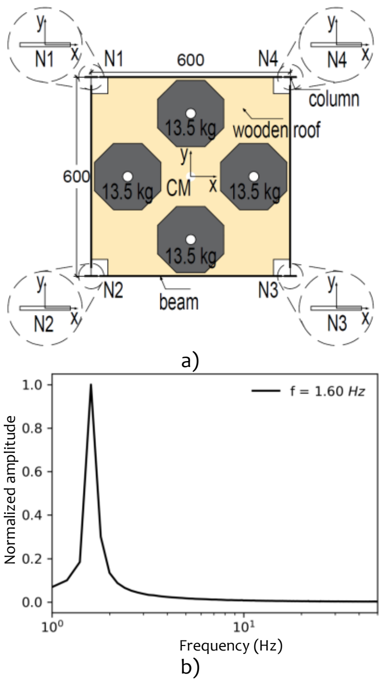

Fig. 6. Specimen E-1. (a) Floor plan diagram of specimen E-1. (b) Natural frequency content of free vibration in the Y direction of specimen E-1.

Fig. 7 shows specimen E-2 and its corresponding frequency content. This specimen features columns with double the thickness at corners N3 and N4 compared to the columns at corners N2 and N1.

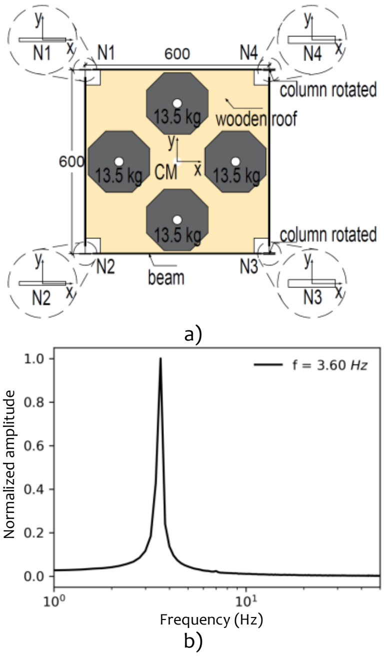

Fig. 7. Specimen E-2. (a) Floor plan diagram of specimen E-2. (b) Natural frequency content of free vibration in the Y direction of specimen E-2.

Fig. 8 shows specimen E-3 with its corresponding frequency content. This specimen features a rotated column at corner N3.

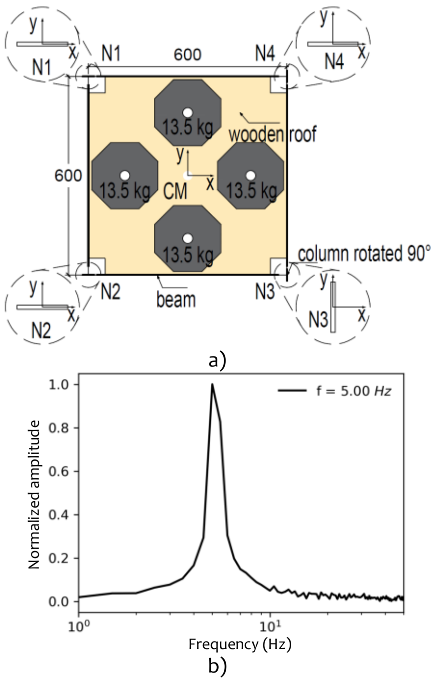

Fig. 8. Specimen E-3. (a) Floor plan diagram of specimen E-3. (b) Natural frequency content of free vibration in the Y direction of specimen E-3.

Fig. 9 shows specimen E-4, which features two rotated columns at corners N3 and N4, respectively.

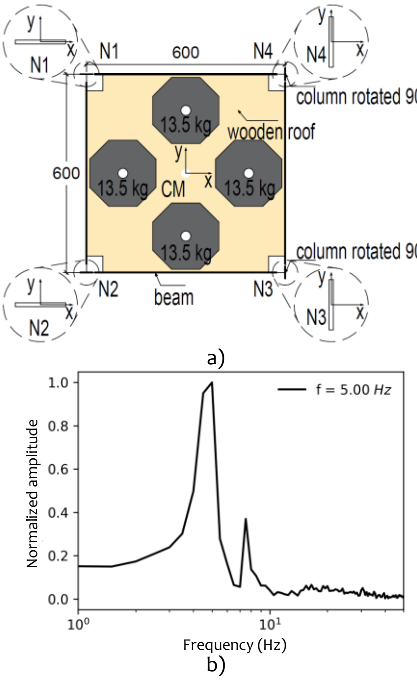

Fig. 9. Specimen E-4. (a) Floor plan diagram of specimen E-4. (b) Natural frequency content of free vibration in the Y direction of specimen E-4.

TABLE V summarizes the properties of the specimens.

TABLE V
Summary of specimen properties

Specimen	f_y (Hz)	T_y (s)	Weight (kg)
E-1	1.60	0.63	70
E-2	3.60	0.28	70
E-3	5.00	0.20	70
E-4	5.00	0.20	70

5.2 MONITORING SCHEME OF SPECIMENS

To monitor the response of the specimens to seismic events generated by the movement of shaking table, displacement and acceleration sensors were used. Fig. 10 and 11 present the side view and top view schematics, respectively. These schematics show the location of displacement sensors and the arrangement of the specimen on the shaking table.

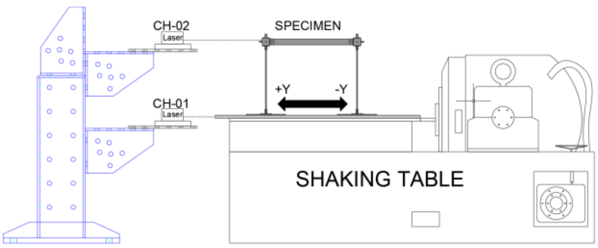

Fig. 10. Testing scheme, side view.

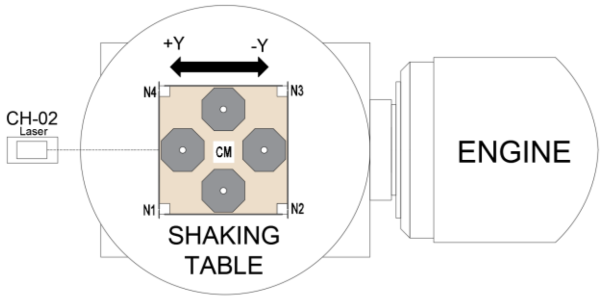

Fig. 11. Testing scheme, top view.

Additionally, TABLE VI presents a list of sensors used to monitor each of the points of interest in the specimens.

TABLE VI
List of sensors installed to monitor the specimens

Type of sensor	Magnitude	Direction	Monitored point
Laser	Disp.	Y	BASE
Laser	Disp.	Y	CM
Accelerometer	Accel.	Y	BASE
Accelerometer	Accel.	X	BASE
Accelerometer	Accel.	Y	CM
Accelerometer	Accel.	X	CM
Accelerometer	Accel.	Y	N1
Accelerometer	Accel.	Y	N2
Accelerometer	Accel.	Y	N3
Accelerometer	Accel.	Y	N4
Accelerometer	Accel.	X	N1
Accelerometer	Accel.	X	N2
Accelerometer	Accel.	X	N3
Accelerometer	Accel.	X	N4

Fig. 12 shows the monitoring system installed on one of the specimens on the shaking table.

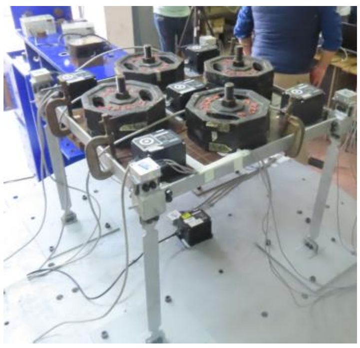

Fig. 12. Monitoring system for specimen on shaking table.

5.3 EXPERIMENTAL PROCEDURE

To carry out the experimental process, seismic records were first defined for incremental dynamic testing. The seismic records used for tests on the shaking table were generated from two historical earthquakes in Peru: the 1974 Lima earthquake and the 2007 Pisco earthquake.

These earthquakes were modified so that the frequency content of each earthquake includes the natural frequencies of the specimens tested. According to free vibration tests, the specimens exhibit frequencies between 1.60 Hz and 5 Hz. However, specimen E-4 exhibits a second natural vibration frequency close to 10 Hz (see Fig. 9b). Therefore, it was decided that the records used for dynamic tests should have a significant frequency content between 1 Hz and 10 Hz.

Fig. 13 shows the modified 1974 Lima earthquake, which was recorded on the base of the shaking table. Fig. 13a displays the record with normalized amplitudes, where the amplitudes of the original record were divided by its maximum amplitude. Additionally, Fig. 13b shows the frequency content of this new signal. This new record is named LIMA-1974.

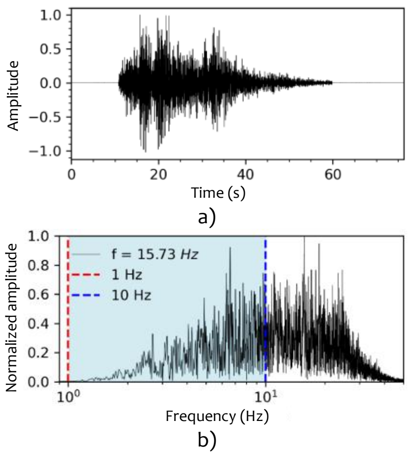

Fig. 13. LIMA-1974 Record. (a) Acceleration record. (b) Frequency content of the seismic record.

Fig. 14 shows the modified 2007 Pisco earthquake, which was recorded on the base of the shaking table. Fig. 14a displays the record with normalized amplitudes, where the amplitudes of the original record were divided by its maximum amplitude. Additionally, Fig. 14b shows the frequency content of this new signal. This new record will be named PISCO-2007.

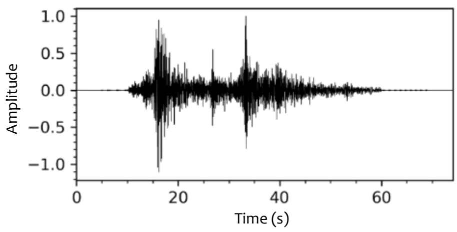

a)

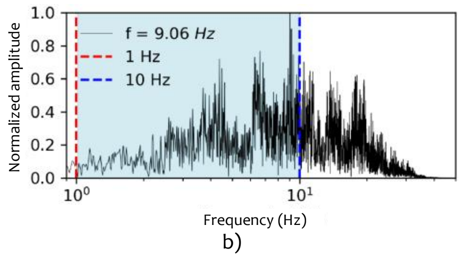

b)

Fig. 14. PISCO-2007 Record. (a) Acceleration record. (b) Frequency content of the seismic record.

It's important to note that there were 2 specimens of each type shown in section 4.1, totaling 8 specimens tested. A group of 4 specimens was subjected to the LIMA-1974 record, and the other group of 4 was subjected to the PISCO-2007 record. The experimental procedure involved incremental dynamic testing, starting with a small amplitude signal on the shaking table and gradually increasing the signal's amplitude until the specimens entered the inelastic range. It's worth noting that the seismic records were applied along the Y direction of the specimens. TABLE VII shows the number of seismic signals to which the 8 specimens were subjected.

TABLE VII
Summary of the number of seismic signals sent in the incremental dynamic tests

Seismic record	Specimen	Number of seismic signals
LIMA-1974	E-1	8
	E-2	10
	E-3	12
	E-4	11
PISCO-2007	E-1	8
	E-2	10
	E-3	12
	E-4	10

5.4 EXPERIMENTAL RESULTS

Fig. 15 shows the flowchart summarizing the procedure for processing the responses obtained during the incremental dynamic tests for each of the specimens.

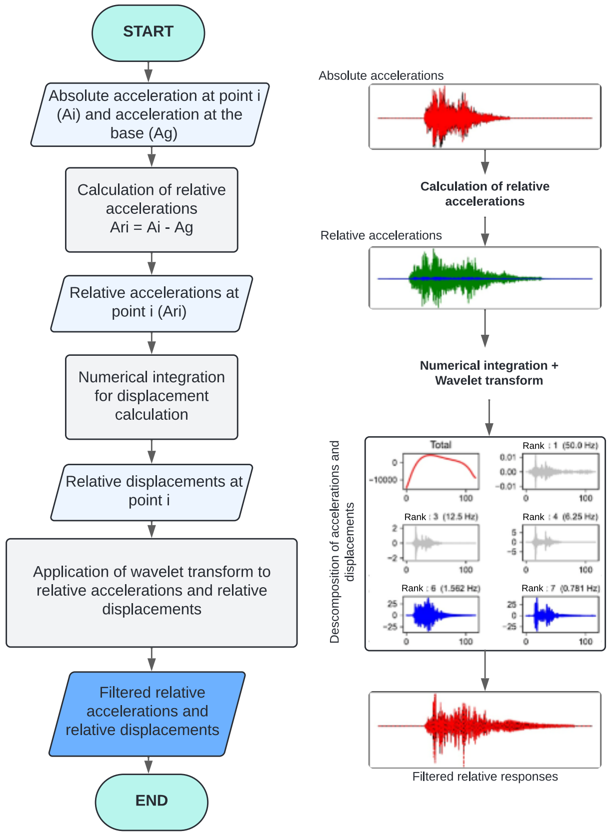

Fig. 15. Flowchart of experimental data processing.

Fig. 16 shows histograms of the experimental parameters calculated from the results of the incremental dynamic tests can be observed. Additionally, in Fig. 17, the distribution of the values of each parameter relative to the degree of torsional irregularity can be observed.

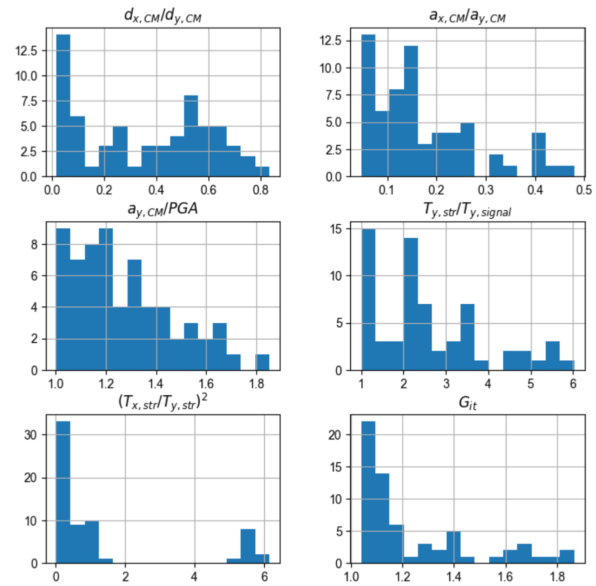

Fig. 16. Histograms of experimental parameters.

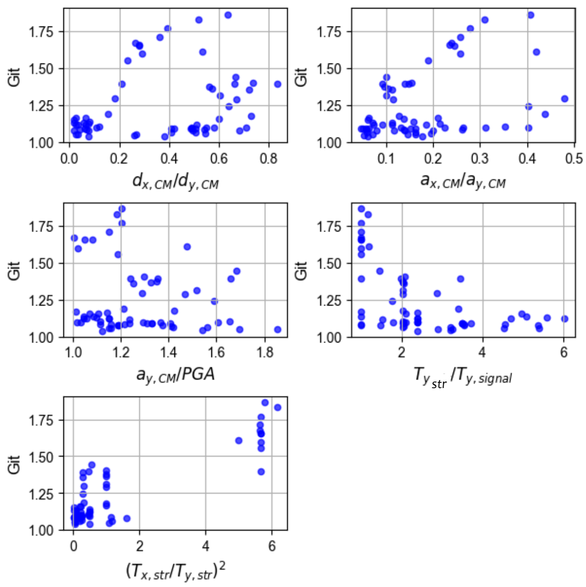

Fig. 17. Relation of G_{it} with the study parameters.

6. PREDICTION MODEL

In this chapter, the development of the machine learning algorithm for predicting the value of G_{it} was carried out. To this end, a random forest model was trained with data obtained from numerical simulations to predict the values of G_{it} for different seismic scenarios. The trained prediction model was adjusted with the experimental parameters obtained to create a hybrid prediction model. Finally, the mathematical formulation of the G_{it} was carried out using the experimental results.

6.1 TRAINING THE PREDICTION MODEL WITH THE RESULTS OF NUMERICAL SIMULATIONS

To develop the prediction model, the Random Forest model was chosen. To understand this model, one must first understand what a Decision Tree model is. According to Géron [13], a Decision Tree model divides the training dataset into several subsets, each containing data points with output values that exhibit little dispersion. In this case, the parameter used to measure the data dispersion in each subset is the Mean squared Error (MSE). Accordingly, Géron [13] states that a Random Forest model is a collection of Decision Trees, where the final prediction value of the Random Forest model is the mode of all predictions made by the decision trees that compose the forest.

To train the Random Forest model with the results of the numerical simulations, the RandomForestRegressor function from Python's scikit-learn library was used. The prediction model consists of 800 decision trees and was trained with 80% of the data, with the remaining 20% used for model validation. The results of this validation can be seen in Fig. 18, which shows the model's prediction results compared to the analysis values. Higher values on the color scale indicate a higher density of points.

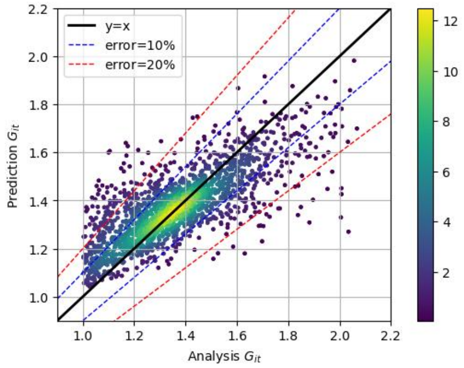

Fig. 18. Comparison between the predicted G_{it} and the analyzed G_{it}.

Fig. 19 shows the distribution of percentage errors of the prediction model.

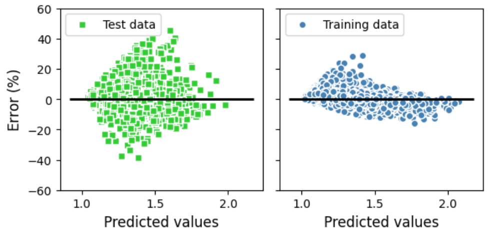

Fig. 19. Prediction model errors.

Likewise, TABLE VIII shows the performance metrics of the prediction model for the calculation of G_{it}:

TABLE VIII
Performance metrics of the prediction model

RMSE	NRMSE (%)	R2
0.135	10.654	0.578

Since the relative displacement of the center of mass is known in each of the analyses, the maximum drifts of the structure can be calculated using the expression $dr_{y,max} = (dr_{y,CM})(G_{it})$. In this expression, the values of the analyzed G_{it} and the predicted G_{it} can be substituted. With this, the values of the analyzed $dr_{y,max}$ and the predicted $dr_{y,max}$ from the prediction model will be obtained. Fig. 20 shows the comparison between these values.

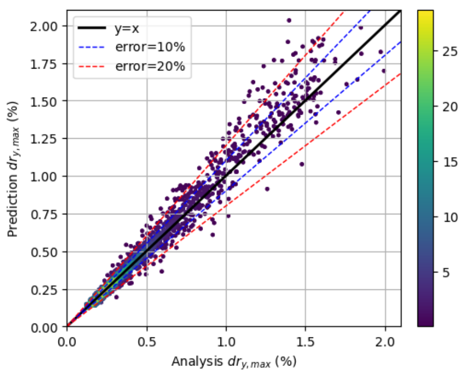

Fig. 20. Comparison between the maximum drifts from analysis and the maximum drifts calculated from the prediction model.

Finally, TABLE IX shows the performance metrics of the final model for the estimation of maximum drifts.

TABLE IX
Performance metrics for estimating maximum drifts from the prediction model

RMSE	NRMSE (%)	R2
0.001	4.054	0.955

6.2 FITTING THE PREDICTION MODEL WITH EXPERIMENTAL RESULTS

After obtaining the response parameters from the experimental study, the prediction model developed in Section 6.1 was recalibrated using the experimental data. Specifically, 40% of the experimental dataset was randomly selected for training, while the remaining 60% was used for validation. This updated model is referred to as the hybrid prediction model, as it was trained on a combined dataset consisting of both numerical simulation and experimental data. The hybridization was achieved by augmenting the original numerical dataset with the experimental data and retraining the model on this expanded database. The process is illustrated in Fig. 21.

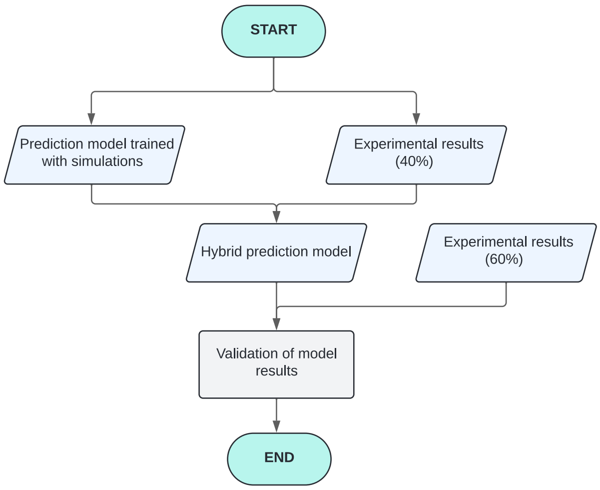

Fig. 21. Flowchart for the creation of the hybrid prediction model.

The results obtained from the evaluation of the hybrid prediction model on the experimental validation results can be observed on Fig.22.

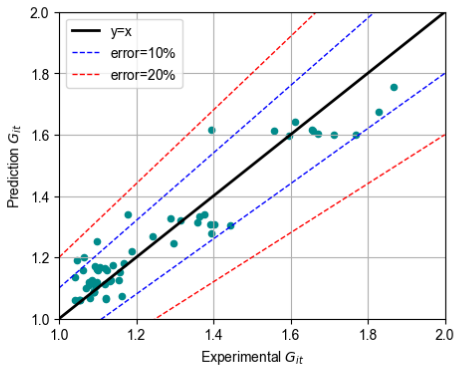

Fig. 22. Comparison between the experimental G_{it} and the predicted G_{it}.

Likewise, TABLE X shows the performance metrics of the prediction model for calculating G_{it}.

TABLE X
Performance metrics of the hybrid prediction model

RMSE	NRMSE (%)	R2
0.09	11.40	0.84

Since the drift of the center of mass is known for each of the dynamic tests, the maximum drifts of the specimens can be calculated using the expression $dr_{y,max} = (dr_{y,CM})(G_{it})$ and compare these experimental values with the calculated values. This comparison is shown in Fig. 23.

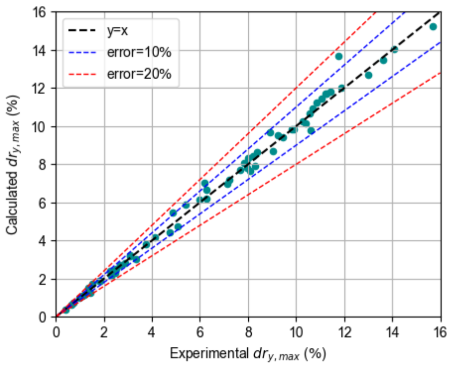

Fig. 23. Comparison between the experimental $dr_{y,max}$ and the $dr_{y,max}$ calculated from the prediction model.

Likewise, TABLE XI shows the performance metrics of the prediction model for calculating $dr_{y,max}$.

TABLE XI
Performance metric of the estimation of maximum drifts from the hybrid prediction model

RMSE	NRMSE (%)	R2
0.005	3.56	0.98

As observed in Fig. 23 and TABLE XI, the values of $dr_{y,max}$ obtained from the prediction model align with the experimental results. However, the disadvantage of the developed prediction model is that it lacks an explicit equation that relates the proposed parameters to G_{it}. Therefore, the next section will propose a formula to calculate G_{it} based on the experimental results.

6.3 MATHEMATICAL EXPRESION OF G_{it}

In this section, a mathematical expression of G_{it} was conducted to establish a relationship between

$$G_{it} = 1 + 0.26\frac{d_{x,CM}}{d_{y,CM}} + 0.21\frac{a_{x,CM}}{a_{y,CM}} + 0.02\frac{T_{y,\,\mathrm{str}}}{T_{y,\,\mathrm{signal}}} + 0.10\left(\frac{T_{x,str}}{T_{y,str}}\right)^2 \quad (6)$$

this variable and the parameters shown in Fig. 16. For this purpose, a multiple linear regression was performed considering G_{it} as the dependent variable. From the linear regression, equation (6) was obtained, which relates G_{it} to the proposed parameters. Note that the parameter $(L/B)^2$ has not been included because it is a constant value equal to one for all tested specimens.

Additionally, Fig. 24 shows the comparison between the experimental G_{it} and the calculated G_{it} with the equation proposed earlier.

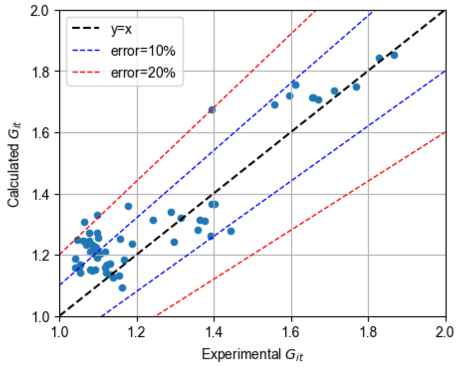

Fig. 24. Comparison between the experimental G_{it} and the calculated G_{it}.

Similarly, TABLE XII shows the performance metrics of the multiple linear regression model for calculating G_{it}:

TABLE XII
Performance metrics of the Mathematical Formulation

RMSE	NRMSE (%)	R2
0.116	14.03	0.73

Since the displacement of the center of mass is known for each of the dynamic tests, the maximum drifts of the specimens can be calculated using the expression $dr_{y,max} = (dr_{y,CM})(G_{it})$and compare these experimental values with the calculated values. This comparison is shown on Fig. 25.

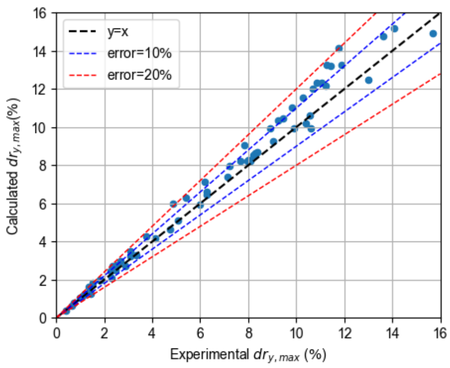

Fig. 25. Comparison between the experimental $dr_{y,max}$ and the calculated $dr_{y,max}$.

Likewise, TABLE XIII shows the performance metrics for the calculation of maximum drifts.

TABLE XIII
Performance metrics for calculating maximum drifts from Mathematical Formulation

RMSE	NRMSE (%)	R2
0.008	5.08	0.964

CONCLUSIONS

A methodology was developed for determining the damage level in buildings with torsional irregularity based on structural and seismic parameters, which were calculated using data obtained from a structural health monitoring system. Seismic simulations of simplified models were conducted to develop the methodology. From the numerical results, a prediction model for the degree of torsional irregularity was developed. The validation of the prediction model was carried out using data obtained from incremental dynamic tests on a shaking table, where test specimens were subjected to multiple seismic records.

-Based on the database created from Dynamic analyses in simplified numerical models, the prediction model for G_{it} was developed, achieving an average absolute error of 6.98%, NRMSE of 10.654%, and R^2 of 0.578. These results allowed for the calculation of maximum drifts with high precision, as NRMSE and R^2 values of 4.054% and 0.955, respectively, were obtained.

-Incremental dynamic experimental tests were conducted in a single direction with different seismic records on metal structures with various degrees of torsion. During these tests, the specimens experienced both elastic and inelastic ranges. Based on the prediction model developed from numerical simulations, a new hybrid prediction mode was adjusted using 40% of the experimental results. This adjusted model was validated with the remaining 60% of experimental data. The results obtained with the prediction model aligned well with the experimental values of G_{it}, yielding NRMSE and R^2 values of 11.40% and 0.84, respectively. Additionally, maximum drifts were calculated with high precision from the predicted value of, resulting in NRMSE and R^2 values of 3.56% and 0.98, respectively.

-A mathematical expression of G_{it} was developed based on the structural and seismic characteristics of the tested specimens. This formulation was proposed using multiple linear regression. Once the calculated values of G_{it} were obtained using the proposed formula, the maximum drifts for each specimen were calculated and compared with the respective experimental results. The proposed method allowed for the accurate calculation of maximum response in structures with torsional irregularity under seismic events, achieving NRMSE and R^2 values of 5.08% and 0.964, respectively.

-The proposed methodology leverages the rapid information provided by structural health monitoring to enable engineers to deliver a faster and more accurate diagnosis of the condition of torsional irregular buildings following an earthquake. This allows authorities or homeowners to make informed decisions regarding the repair or demolition of the building based on its condition.

RECOMMENDATIONS

-The tool proposed in this research could be incorporated into the 'Post-Earthquake Evaluation of Structures' section of the technical standard E.030-2018 of the Peruvian National Building Code, with the aim of enabling a more accurate damage assessment in structures with plan torsional irregularity.

-The proposed methodology could be applied to more complex structures than those analyzed in this study as a rapid preliminary diagnostic tool. However, it is recommended that structural engineers perform a more detailed analysis to fully understand the response of such irregular structures. This could be achieved by monitoring additional points across the floor plan to better assess structural rotation during an earthquake.

- The proposed methodology is based on the analysis of seismic records with predominant frequencies ranging from 0.33 to 17.68 Hz, as shown in Table II. These records originate from various regions of Peru, covering a wide spectrum of frequency content. Since the predictive equation incorporates the ratio between the structural period and the predominant period of the seismic record $\frac{T_{y,\,\text{str}}}{T_{y,\,\text{signal}}}$, it is recommended to apply the model using seismic inputs whose predominant periods fall within the range analyzed in this study. Applying the model to records outside this range may result in reduced accuracy or reliability.

-Regarding soil type, although it was not explicitly considered in the model, its influence is inherently reflected in the frequency content of the ground motion. Therefore, the model can be applied to buildings on different soil types, provided the predominant period of the seismic record falls within the specified range.

ACKNOWLEDGEMENTS

The authors would like to thank the Faculty of Civil Engineering at the National University of Engineering and the Structures Laboratory at Japan-Peru Center for Earthquake Engineering Research and Disaster Mitigation (CISMID). Special thanks to National Budget PP-0068, the Program for the Reduction of Vulnerability and Emergency Response to Disasters - PREVAED.

REFERENCES

[1] N. Pulido *et al.*, "Scenario Source Models and Strong Ground Motion for Future Mega-earthquakes: Application to Lima, Central Peru," *Bulletin of the Seismological Society of America*, vol. 105, no. 1, pp. 368–386, Feb. 2015, doi: 10.1785/0120140098.

[2] A. Ibrahim, A. Eltawil, Y. Na, and S. El-Tawil, "A Machine Learning Approach for Structural Health Monitoring Using Noisy Data Sets," *IEEE Trans. Automat. Sci. Eng.*, vol. 17, no. 2, pp. 900–908, Apr. 2020, doi: 10.1109/TASE.2019.2950958.

[3] C. Gonzales *et al.*, "Preliminary System for the Estimation of Peak Ground Acceleration Distribution in Metropolitan Lima

and Callao: Application in Recent Seismic Events," *JDR*, vol. 18, no. 4, pp. 319–328, Jun. 2023, doi: 10.20965/jdr.2023.p0319.

[4] H. Gokdemir, H. Ozbasaran, M. Dogan, E. Unluoglu, and U. Albayrak, "Effects of torsional irregularity to structures during earthquakes," *Engineering Failure Analysis*, vol. 35, pp. 713–717, Dec. 2013, doi: 10.1016/j.engfailanal.2013.06.028.

[5] Y. Bozorgnia and W. K. Tso, "Inelastic earthquake response of asymmetric structures," *Journal of Structural Engineering*, vol. 112, no. 2, pp. 383-400, Feb. 1986, doi: 10.1061/(ASCE)0733-9445(1986)112:2(383).

[6] A. K. Chopra and R. K. Goel, "Effects of plan asymmetry in inelastic seismic response of one-story systems," *Journal of Structural Engineering*, vol. 117, no. 5, pp. 1492–1513, May 1991, doi: 10.1061/(ASCE)0733-9445(1991)117:5(1492).

[7] K. M. Alaa, K. F. El-Kashif, and H. M. Salem, "New definition for torsional irregularity based on floor rotations of reinforced concrete buildings," *Journal of Engineering and Applied Science*, vol. 69, no. 12, 2022, doi: 10.1186/s44147-021-00061-5.

[8] B. K. Oh, B. Glisic, S. W. Park, and H. S. Park, "Neural network-based seismic response prediction model for building structures using artificial earthquakes," *Journal of Sound and Vibration*, vol. 468, p. 115109, Mar. 2020, doi: 10.1016/j.jsv.2019.115109.

[9] J. Jaramillo, M. Diaz, C. Zavala, K. Kusunoki, I. Inocente, and D. Otero, "Wavelet Transform Method for the Evaluation of the Seismic Response of One Isolated Building in the Lima Metropolitan Area," *JDR*, vol. 18, no. 4, pp. 338–349, Jun. 2023, doi: 10.20965/jdr.2023.p0338.

[10] K. A. O. Galindo, "Evaluación del efecto de la simultaneidad de las componentes de sismo en estructuras con irregularidad torsional," Thesis, Universidad Nacional de Ingeniería, Lima, 2019.

[11] T. Suzuki, A. Puranam, K. Elwood, H. Lee, F. Hsiao, and S. Hwang, "Shake table tests of seven-story reinforced concrete structures with torsional irregularities: Test program and datasets," Earthquake Spectra, vol. 37, no. 4, pp. 2946–2970, 2021, doi: 10.1177/87552930211016869.

[12] S. Raschka, Y. Liu, and V. Mirjalili, *Machine Learning with PyTorch and Scikit-Learn,* Packt Publishing, 1st ed., Feb. 2022, ISBN 978-1-80181-931-2.

[13] A. Géron, *Hands-on Machine Learning with Scikit-Learn, Keras, and TensorFlow Concepts, Tools, and Techniques to Build Intelligent Systems SECOND EDITION*, 2nd ed. O'Reilly Media, 2019, ISBN 978-1-492-03264-9.